Applied Physics Letters

Ultraviolet waveband vector beams generation assisted by the nonlinear frequency conversion

Cite as: Appl. Phys. Lett. **119**, 011104 (2021); https://doi.org/10.1063/5.0053781
Submitted: 11 April 2021 . Accepted: 17 June 2021 . Published Online: 06 July 2021

Hui Li, Haigang Liu, Yangfeifei Yang, Ruifeng Lu, and Xianfeng Chen

Applied Physics Letters ARTICLE scitation.org/journal/apl

Ultraviolet waveband vector beams generation assisted by the nonlinear frequency conversion

Cite as: Appl. Phys. Lett. **119**, 011104 (2021); doi: 10.1063/5.0053781
Submitted: 11 April 2021 · Accepted: 17 June 2021 ·
Published Online: 6 July 2021

Hui Li,[1,2] Haigang Liu,[2] Yangfeifei Yang,[2] Ruifeng Lu,[1,a] and Xianfeng Chen[2,3,4,5,a]

AFFILIATIONS

[1]Department of Applied Physics, Nanjing University of Science and Technology, Nanjing 210094, China
[2]State Key Laboratory of Advanced Optical Communication Systems and Networks, School of Physics and Astronomy, Shanghai Jiao Tong University, Shanghai 200240, China
[3]Shanghai Research Center for Quantum Sciences, Shanghai 201315, China
[4]Jinan Institute of Quantum Technology, Jinan 250101, China
[5]Collaborative Innovation Center of Light Manipulations and Applications, Shandong Normal University, Jinan 250358, China

[a)]**Authors to whom correspondence should be addressed:** rflu@njust.edu.cn and xfchen@sjtu.edu.cn

ABSTRACT

Vector beams with a nonseparable polarization distribution are almost thoroughly studied from their generation to application in infrared and visible regimes. Until now, the nonlinear generation of ultraviolet vector beams is only focused on the nonlinear optical processes of gas molecules, which seriously impacts its further applications due to the unstable property. Here, we present a study on the generation of ultraviolet vector beams assisted by the nonlinear frequency conversion processes in potassium dihydrogen phosphate crystals. The vectorial properties of the generated ultraviolet waveband vector beams are characterized in both theoretical and experimental environments. The proposed method paves the way for the generation of extreme ultraviolet vector beams with solid-state nonlinear crystal, which is a more compact and stable way compared with the gas nonlinear method. This work also opens a route for photolithographic techniques and laser processing based on ultraviolet waveband vector beams.

Vector beams with the space-variant polarization distribution in the transverse plane provide powerful capabilities for applications in diverse areas of science and technology, such as high-resolution imaging[1] and laser processing.[2] From a historical perspective, research on vector beams or rather the special category of cylindrically symmetric vector beams could be traced back to the early 1960s, when Snitzer put forward the concept of the vectorial optical field.[3] Thereafter, Pohl published the original experimental work that opened up the research on vector beams.[4] In recent years, as an important research topic, numerous spatial-variant polarization vector beams, e.g., radial, azimuthal, and spiral polarization distributions, have been reported.[5–16] Lights with radially and azimuthally polarized distributions are paradigms of vector beams. On the one hand, the radially polarized beams are particularly interesting for a strong nonvanishing longitudinal field below the diffraction limit upon focusing by high-NA objectives.[5–7] This property is of great significance in the fields of optical trapping,[8–12] laser micromachining,[2,13] vector light microscopy,[1,14] and so on. Furthermore, the radially polarized beams have also been shown to be relevant in the area of quantum communications to improve the communication capacity.[15] On the other hand, the azimuthally polarized beams provide a higher image quality and show a better trapping efficiency.[17–19] Due to its unique properties of nonuniform polarization structures, vector beams also present promising applications in the field of metrology.[20–23] As prominent examples, such vector beams can be applied as an advanced optical sensing tool to track fast moving objects in two dimensions in real time[21] as well as to perform single-shot polarization-dependent measurements and experimental preparation of the samples with position-dependent spin at atomic scale.[22,23]

To date, several methods have been proposed to produce the vector beams in the infrared-visible regime in the linear optical field. By using the intracavity axicon,[24] birefringence of the gain media,[4] conical pump beams,[25] or geometric phase control,[26,27] laser cavities can be customized to generate cylindrical vector beams. The external cavity techniques to generate vector beams have been demonstrated by means of an interference approach[28] or by using π-cylindrical lens mode converters,[29] q-plates,[11] spatial liquid modulators,[12] photo-patterned liquid crystals,[30] digital micromirrors devices,[31] and optical fibers.[32] However, the spectral limitation of those modulation devices

mentioned above prevents the nonlinear generation of vector beams in the ultraviolet regime, which is highly desired in fields of laser machining and lithography in the nanometer resolution. Although the high-order harmonic generation of gases can be applied to generate the ultraviolet waveband vector beam, it always has a relatively low conversion efficiency and signal-to-noise ratio.[33] On the contrary, solid-state crystals are more stable and have a relatively higher conversion efficiency in nonlinear optical processes. Therefore, it is necessary for the solid-state nonlinear crystal to have appropriate properties that can directly generate the ultraviolet vector beams. In recent years, vector beams have been successfully converted from the infrared to visible regime based on two cascading crystals whose fast axes are arranged elaborately perpendicular to each other[34–36] or combined with a Sagnac loop.[37,38]

In this paper, we propose a method to achieve ultraviolet waveband vector beams by using solid-state crystals through nonlinear optical processes. In our experiment, the ultraviolet vector beams can be achieved by using sum-frequency generation (SFG) processes of infrared vector beams and a frequency doubled Gaussian beam. First, we experimentally verify the generation of vector beams in infrared and ultraviolet regimes with a topological charge varying from 1 to 3. Then, the polarization states of the generated ultraviolet vector beams are measured in the experiment, which are in accordance with the theoretical ones. Furthermore, the relative mode weightage of the orthogonal components of the generated ultraviolet vector beams is measured. Finally, we measure the conversion efficiency during the nonlinear optical processes.

The experimental setup is displayed in Fig. 1. A high-energy diode-pumped all-solid-state Q-switched laser with the wavelength of 1064 nm, the repetition frequency of 1 kHz, and the pulse duration of 10 ns is utilized as the light source. A Glan–Taylor prism is used to initialize the polarization direction of the fundamental frequency (FF) light to the horizontal direction. To adjust the polarization states of the FF wave, a half wave plate (HWP_1) combined with a quarter wave plate (QWP_1) with its fast axis along –45° with respect to the horizontal direction is employed. The first step is to separate the two

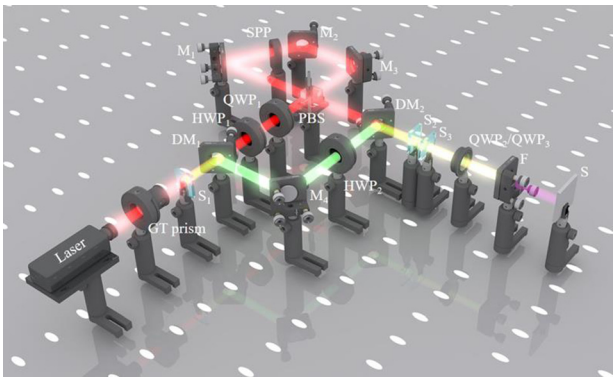

FIG. 1. Schematic of the experimental setup. GT prism, Glan–Taylor prism; HWP_1 and HWP_2, half wave plates operate at 1064 and 532 nm, respectively; DM_1 and DM_2, dichroic mirror; QWP_1, QWP_2, and QWP_3, quarter wave plates with the operating wavelength of 1064, 1064, and 355 nm, respectively; PBS, polarized beam splitter; M_1, M_2, M_3, and M_4, mirrors; SPP, spiral phase plate; S_1, 5 mol. % $MgO:LiNbO_3$; S_2 and S_3, potassium dihydrogen phosphate crystals; F, filter; S, screen.

polarization components into two counterpropagating beams by using a polarizing beam splitter (PBS). After passing through a Sagnac loop, which is composed of three mirrors (M_1, M_2, and M_3) and a spiral phase plate (SPP), beams with an opposite topological charge in two orthogonal polarization states are generated. Two orthogonal beams are recombined by the PBS where the FF beam can be expressed the cylindrical coordinate system (ρ, φ, z) in the form of

$$E_1(\rho,\varphi,z) = A_1 \begin{pmatrix} \exp\left[i(l\varphi+\delta+2\gamma+k_z z)\right] \\ i\exp\left[-i(l\varphi+2\gamma+k_z z)\right] \end{pmatrix}. \quad (1)$$

Here, $E_1(\rho,\varphi,z)$ represents the FF beam with a wavelength of 1064 nm. A_1, l, and φ describe the amplitude, topological charge, and azimuthal angle, respectively. δ is the phase difference of the Sagnac loop, which is caused by the reflection of mirrors, γ refers to the angle between the fast axis of HWP_1 and the horizontal direction, k_z is the wave vector along the propagation direction. Then, QWP_2 with an operating wavelength of 1064 nm is used to convert the FF beam into vector beams. After passing through these optical elements, the vector beams corresponding to 1064 nm are generated and recorded by a charge coupled device (CCD). In another path, a nonlinear crystal S_1 (5 mol. % $MgO:LiNbO_3$) is arranged to get the second harmonic (SH) beams. S_1 is cut for the type-I (oo-e) phase matching condition; thus, the SH beams can be easily generated with a single FF beam. The angle between the propagation direction and optical axis of the crystal is 75° according to the Sellmeier equation.[39] A dichroic mirror (DM_1) is used to reflect the SH beam and selectively pass FF beam. M_4 and the other dichroic mirror (DM_2) are used to combine the FF and SH beams together. We insert a half wave plate (HWP_2) into the SH beam arm with its fast axis orienting at 22.5° to rotate the vertical polarization to the 45° direction. Two cascading nonlinear crystals (S_2 and S_3) with the thickness of 3 mm are inserted between the DM_2 and QWP_2. Both samples are potassium dihydrogen phosphate (KDP) crystals whose fast axes are arranged perpendicular to each other. The optical axis angle of the KDP crystal is fixed at 59.3° with respect to the propagation direction to fulfill the type-II (eo-e) phase matching condition. Thus, the horizontal and vertical components of FF beams separately take part in the SFG, generating the 355 nm beams with horizontal and vertical components, respectively. Under the undepleted pump and paraxial approximation, the coupled wave equation that describes the generated SFG can be written as

$$\frac{dE_3(\rho,\varphi,z)}{dz} = \frac{2i\omega_3^2 d_{eff}}{k_3 c^2} E_1(\rho,\varphi,z)\cdot E_2(\rho,\varphi,z), \quad (2)$$

where $E_3(\rho,\varphi,z)$ represents the sum-frequency (SF) beam with a wavelength of 355 nm. E_2 denotes the SH beam, which can be expressed as $E_2(\rho,\varphi,z) = A_2\begin{pmatrix}1\\1\end{pmatrix}$, where A_2 is the amplitude of the SH beam. ω_3 and k_3, respectively, refer to the angular frequency and wave vector of the SF beam. d_{eff} describes the effective nonlinear coefficient, and c is the light speed in vacuum. Using Eqs. (1) and (2), the generated SF beam can be expressed as

$$E_3(\rho,\varphi) = A_1 A_2 \frac{2i\omega_3^2 d_{eff} L}{k_3 c^2} \begin{pmatrix} \exp\left[i(l\varphi+\delta+\xi+2\gamma)\right] \\ i\exp\left[-i(l\varphi+2\gamma)\right] \end{pmatrix}. \quad (3)$$

Here, ξ is the phase difference between two orthogonal components of the generated 355 nm beams. L is the thickness of the nonlinear crystal

along the propagation direction. As QWP_2 only operates as $\lambda/4$ plate at 1064 nm, it is replaced with the other quarter wave plate (QWP_3), which is operated at 355 nm, and its fast axis has a polarization angle of 45° with respect to the horizontal direction to convert the SF beam into vector beam. The generated ultraviolet vector beam can be expressed as

$$E_3(\rho, \varphi) = A_3 \begin{pmatrix} \cos(l\varphi + \delta/2 + \xi/2 + 2\gamma) \\ \sin(l\varphi + \delta/2 + \xi/2 + 2\gamma) \end{pmatrix}, \quad (4)$$

where A_3 describes the amplitude of the E_3. A filter (F) is used to obstruct FF and SH beams. Limited by the wavelength and lower detection efficiency of the CCD in an ultraviolet waveband, the generated ultraviolet vector beams are recorded on a screen (S).

To confirm the working mechanism of SFG processes, we study the polarization and intensity distribution of the infrared and ultraviolet beams with a topological charge varying from 1 to 3. The experimental results are shown in Fig. 2. We initially set $\delta/2 + \xi/2 + 2\gamma = 0$ by rotating the polarization angle of HWP_1 (γ); hence, the equation describing FF vector beams is simplified as $E_1 = A'_1 \begin{pmatrix} \cos(l\varphi) \\ \sin(l\varphi) \end{pmatrix}$. A'_1 refers to the amplitude of the FF vector beams. The corresponding generated ultraviolet vector beams can be expressed as $E_3(\rho, \varphi) = A_3 \begin{pmatrix} \cos(l\varphi) \\ \sin(l\varphi) \end{pmatrix}$. In this case, the first row in Fig. 2 describes the polarization distribution of the generated vector beams. Figures 2(a)–2(c), respectively, display the FF vector beams with a topological charge $l = 1, 2, 3$, and the corresponding SF vector beams are presented in Figs. 2(d)–2(f). In the experiment, all of the vector beams have a polarization singularity at the center of the optical field. The radius of the hollow spots of the vector beams has a relationship with the topological charge, which can be expressed as $r \propto \sqrt{l}$.[40] As shown in Fig. 2, we can clearly observe that the radius of the hollow spots increases as the topological charge increases.

To examine the spatial polarization distribution of the generated ultraviolet vector beams, a GT prism is inserted between the filter and the screen. The simulated results of topological charge $l = 1, 2, 3$ with different transmission direction (0°, 30°, 60°, 90°, 120°) of GT prism are displayed in the odd rows in Fig. 3. The arrows at the lower right corner of each figure indicate the polarization direction of the GT prism. As shown in the first row of Fig. 3, we observe two clear lobes and the orientation of them is parallel to the transmission direction of the GT prism, confirming that the generated ultraviolet beam is a radially polarized vector beam. With the increase in the topological charge, the vector beams split into $2l$ lobes. The extinction directions rotate anticlockwise as the orientation angle of the optical axis of GT prism gradually changes from 0° to 120° in a 30° interval, as shown in Figs. 3(a1)–3(a5), 3(c1)–3(c5), and 3(e1)–3(e5). The corresponding experimental results are displayed in Figs. 3(b1)–3(b5), 3(d1)–3(d5), and 3(f1)–3(f5), respectively. Experimental results are almost consistent

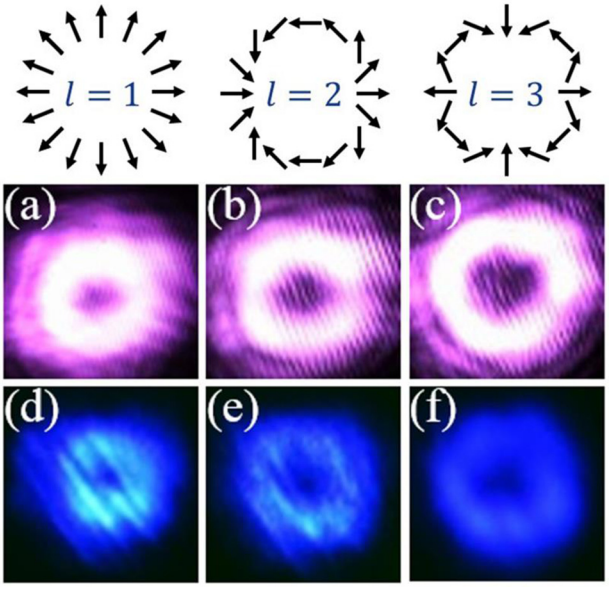

FIG. 2. Experimental results of the polarization and intensity distribution of the generated vector beams. The first row describes the polarization distribution; the middle row is the FF vector beams with topological charge $l = 1, 2, 3$. The corresponding generated SF ultraviolet vector beams are displayed in the bottom row.

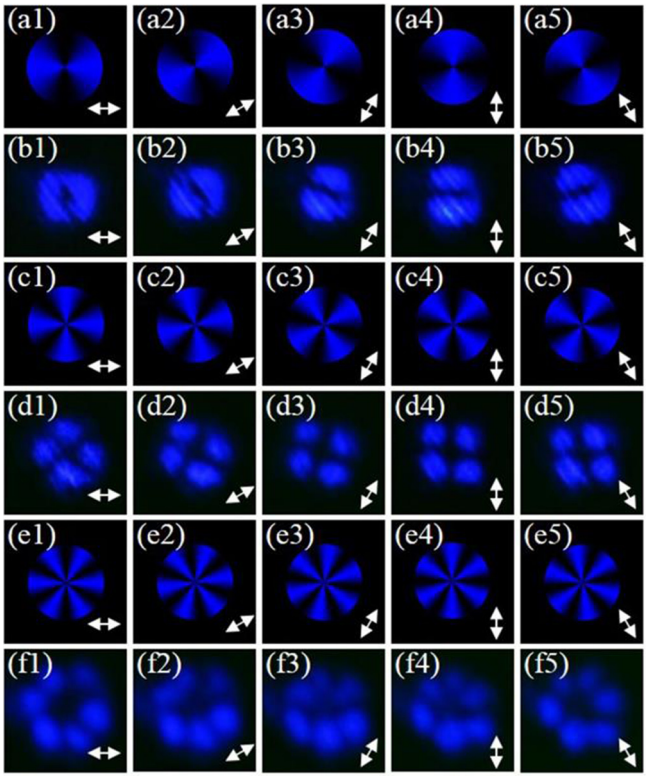

FIG. 3. (a1)–(a5), (c1)–(c5), (e1)–(e5), respectively, represent the simulated intensity profiles of the ultraviolet vector beams with the topological charge of $l = 1, 2, 3$ when the GT prism has different polarization angles (0°, 30°, 60°, 90°, 120°) with respect to the horizontal direction. The corresponding experimental results are shown in (b1)–(b5), (d1)–(d5), (f1)–(f5), respectively. Arrows in the lower right corner of the figures show the polarization angles of the GT prism with respect to the horizontal direction.

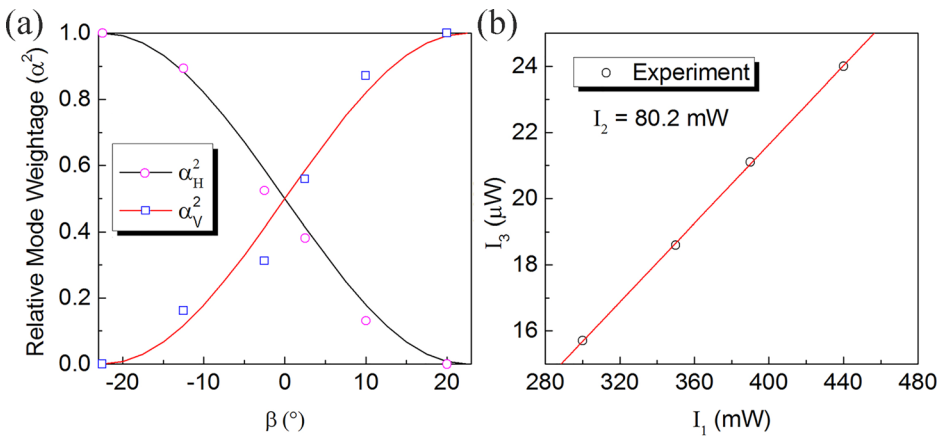

FIG. 4. (a) Simulated (solid lines) and experimental (dots) variation of the relative mode weightage of horizontal and vertical components of SF beams with the topological charge $l = 1$ as the variation of β. (b) Dependence of the generated ultraviolet vector beam intensity (I_3) on the FF beam (I_1) with the topological charge $l = 1$, and the intensity of the SH beam (I_2) equals to 80.2 mW. The dots are the experimental results, and the solid line indicates linear dependency.

with theoretical ones, and the measured intensity distributions reveal the cylindrical polarization property of the generated vector beams.

We further study the relative mode weightage of the generated SF vector beams with the rotation of HWP_1. The generated SF beams can be expressed as $E_3 = \alpha_H|E_{SF}^H\rangle + \alpha_V|E_{SF}^V\rangle$, where α_H and α_V are the relative mode weightage of the horizontal and vertical components. E_{SF}^H and E_{SF}^V represent the horizontal and vertical components of the generated SF beams with the topological charge $l = 1$. Here, $\beta = \delta/4 + \xi/4 + \gamma - \pi/8$. As shown in Fig. 4(a), the experimental results are in close agreement with the simulated ones. By calculation, the average polarization purity corresponding to the ratio of power is approximately 96%. Moreover, we also study the power variation trend of an ultraviolet beam with the increase in the FF power as the topological charge is 1. In the experiment, we insert an attenuator between QWP_1 and PBS to adjust the intensity of the FF beams while SH beams keeps invariable. The formula of conversion efficiency can be expressed as $\eta \propto CI_3/I_1$, where I_1 and I_3 are the intensities of the FF and SF vector beams, respectively, and C is a constant. As an evident from Fig. 4(b), the intensity of the generated ultraviolet vector beam increases linearly to the intensity of the FF beam. The intensity of the SH beam is 80.2 mW. Thus, the conversion efficiency from FF and SH beams to current SF beams is about $0.65‰\ W^{-1}$ in the case of $l = 1$. The conversion efficiency of the Gaussian beams in SFG process is about $1.17‰\ W^{-1}$.

We would like to point out that the vector beams could be produced in the ultraviolet region by combining solid-state nonlinear crystals through nonlinear optical processes. In this way, the polarization distribution can be easily adjusted by rotating the axis of the HWP_1 or changing the topological charge of SPP. Most importantly, this method opens a route to get an ultraviolet vector beam laser source, which will promote the precision and efficiency of the laser processing.

In conclusion, we have both experimentally and theatrically demonstrated the generation of vector beams in the ultraviolet region by utilizing solid-state crystals. In our experiment, ultraviolet vector beams with the topological charge $l = 1, 2, 3$ are generated and their vectorial properties are demonstrated in both simulated and experimental environments. The experimental results match well with the theoretical ones. Then, the relative mode weightage of the orthogonal components of the generated 355 nm vector beams is measured. Moreover, the relationship between the intensity of SF beam and the FF beam is studied. The results show that the intensity of SF beams varies linearly with the FF beams. The method proposed here may provide a solid-state and compact way to produce vector beams with much shorter wavelength. The generated cylindrical vector beams with a donut-intensity profile and controllable polarization distribution, thus, offer advantages in photolithographic techniques, superfocusing, optical metrology, etc.

This work was supported in part by the National Key Research and Development Program of China under Grant Nos. 2017YFA0303700 and 2018YFA0306301, National Natural Science Foundation of China under Grant Nos. 11734011 and 12004245, the Foundation for Shanghai Municipal Science and Technology Major Project under Grant No. 2019SHZDZX01-ZX06, Shandong Quancheng Scholarship under Grant No. 00242019024, and China Postdoctoral Science Foundation under Grant No. 2021M691601.

AUTHORS' CONTRIBUTIONS

H. Li and H. Liu contributed equally to this work.

DATA AVAILABILITY

The data that support the findings of this study are available within this article.

REFERENCES

[1]G. Bautista and M. Kauranen, ACS Photonics **3**, 1351 (2016).
[2]R. Drevinskas, J. Zhang, M. Beresna, M. Gecevicius, A. Kazanskii, Y. Svirko, and P. Kazansky, Appl. Phys. Lett. **108**, 221107 (2016).
[3]E. Snitzer, J. Opt. Soc. Am. **51**, 491 (1961).
[4]D. Pohl, Appl. Phys. Lett. **20**, 266 (1972).
[5]Y. Zhao and J. Wang, Opt. Lett. **40**, 4843 (2015).
[6]Q. Zhan and J. R. Leger, Opt. Express **10**, 324 (2002).
[7]R. Dorn, S. Qubis, and G. Leuchs, Phys. Rev. Lett. **91**, 233901 (2003).
[8]Y. Zhang, P. Chen, S. Ge, T. Wei, J. Tang, W. Hu, and Y. Lu, Appl. Phys. Lett. **117**, 081101 (2020).
[9]C. Min, Z. Shen, J. Shen, Y. Zhang, H. Fang, G. Yuan, L. Du, S. Zhu, T. Lei, and X. Yuan, Nat. Commun. **4**, 2891 (2013).
[10]R. Xu, P. Chen, J. Tang, W. Duan, S. Ge, L. Ma, R. Wu, W. Hu, and Y. Lu, Phys. Rev. Appl. **10**, 034061 (2018).
[11]P. Chen, W. Ji, B. Y. Wei, W. Hu, V. Chigrinov, and Y. Lu, Appl. Phys. Lett. **107**, 241102 (2015).

[12]X. Wang, J. Chen, Y. Li, J. Ding, C. Guo, and H. Wang, Phys. Rev. Lett. **105**, 253602 (2010).
[13]C. Hnatovsky, V. Shvedov, W. Krolikowski, and A. Rode, Phys. Rev. Lett. **106**, 123901 (2011).
[14]A. F. Abouraddy and K. Toussaint, Phys. Rev. Lett. **96**, 153901 (2006).
[15]B. Ndagano, I. Nape, M. Cox, C. Rosales-Guzman, and A. Forbes, J. Lightwave Technol. **36**, 292 (2018).
[16]Y. Pan, Y. Li, S. Li, Z. Ren, Y. Si, C. Tu, and H. Wang, Opt. Lett. **38**, 3700 (2013).
[17]Y. Kozawa and S. Sato, Opt. Express **18**, 10828 (2010).
[18]S. Hell, Science **316**, 1153 (2007).
[19]R. Chen, K. Agarwal, C. Sheppard, and X. Chen, Opt. Lett. **38**, 3111 (2013).
[20]M. Neugebauer, P. Woźniak, A. Bag, G. Leuchs, and P. Banzer, Nat. Commun. **7**, 1 (2016).
[21]C. Rosales-Guzmán, N. Hermosa, A. Belmonte, and J. Torres, Opt. Lett. **39**, 5415 (2014).
[22]F. Fatemi, Opt. Express **19**, 25143 (2011).
[23]C. Rosales-Guzmán, B. Ndagano, and A. Forbes, J. Opt. **20**, 123001 (2018).
[24]J. Bisson, J. Li, K. Ueda, and Y. Senatsky, Opt. Express **14**, 3304 (2006).
[25]Y. Kozawa and S. Sato, Opt. Lett. **30**, 3063 (2005).
[26]D. Naidoo, F. Roux, A. Dudley, I. Litvin, B. Piccirillo, L. Marrucci, and A. Forbes, Nat. Photonics **10**, 327 (2016).
[27]M. Sakakura, Y. Lei, L. Wang, Y. Yu, and P. G. Kazansky, Light **9**, 1 (2020).
[28]B. Jia, X. Gan, and M. Gu, Opt. Express **13**, 6821 (2005).
[29]G. Milione, S. Evans, D. Nolan, and R. Alfano, Phys. Rev. Lett. **108**, 190401 (2012).
[30]P. Chen, Y. Lu, and W. Hu, Liq. Cryst. **43**, 2051 (2016).
[31]L. Gong, Y. Ren, W. Liu, M. Wang, M. Zhong, Z. Wang, and Y. Li, J. Appl. Phys. **116**, 183105 (2014).
[32]B. Lim, P. Phua, W. Lai, and M. Hong, Opt. Lett. **33**, 950 (2008).
[33]C. Hernández-García, A. Turpin, J. Román, A. Picón, R. Drevinskas, A. Cerkauskaite, P. Kazansky, C. Durfee, and Í. J. Sola, Optica **4**, 520 (2017).
[34]H. Liu, H. Li, Y. Zheng, and X. Chen, Opt. Lett. **43**, 5981 (2018).
[35]L. Zhang, X. Qiu, F. Li, H. Liu, X. Chen, and L. Chen, Opt. Express **26**, 11678 (2018).
[36]H. Li, H. Liu, and X. Chen, Appl. Phys. Lett. **114**, 241901 (2019).
[37]C. Yang, Z.-Y. Zhou, Y. Li, Y.-H. Li, S.-L. Liu, S.-K. Liu, Z.-H. Xu, G.-C. Guo, and B.-S. Shi, Opt. Lett. **44**, 219 (2019).
[38]H.-J. Wu, B. Zhao, C. Rosales-Guzmán, W. Gao, B.-S. Shi, and Z.-Z. Zhu, Phys. Rev. Appl. **13**, 064041 (2020).
[39]O. Gayer, Z. Sacks, E. Galun, and A. Arie, Appl. Phys. B **91**, 343 (2008).
[40]N. Bloch, K. Shemer, A. Shapira, R. Shiloh, I. Juwiler, and A. Arie, Phys. Rev. Lett. **108**, 233902 (2012).